BMC Cancer

RESEARCH Open Access

The BET PROTAC inhibitor GNE-987 displays anti-tumor effects by targeting super-enhancers regulated gene in osteosarcoma

Di Wu[1†], Hongli Yin[1†], Chun Yang[1†], Zimu Zhang[1], Fang Fang[1], Jianwei Wang[1], Xiaolu Li[1], Yi Xie[1], Xiaohan Hu[1], Ran Zhuo[1], Yanling Chen[1], Juanjuan Yu[1], Tiandan Li[1], Gen Li[1*] and Jian Pan[1*]

Abstract

Background Osteosarcoma (OS) is one of the most common primary malignant tumors of bone in children, which develops from osteoblasts and typically occurs during the rapid growth phase of the bone. Recently, Super-Enhancers(SEs)have been reported to play a crucial role in osteosarcoma growth and metastasis. Therefore, there is an urgent need to identify specific targeted inhibitors of SEs to assist clinical therapy. This study aimed to elucidate the role of BRD4 inhibitor GNE-987 targeting SEs in OS and preliminarily explore its mechanism.

Methods We evaluated changes in osteosarcoma cells following treatment with a BRD4 inhibitor GNE-987. We assessed the anti-tumor effect of GNE-987 in vitro and in vivo by Western blot, CCK8, flow cytometry detection, clone formation, xenograft tumor size measurements, and Ki67 immunohistochemical staining, and combined ChIP-seq with RNA-seq techniques to find its anti-tumor mechanism.

Results In this study, we found that extremely low concentrations of GNE-987(2–10 nM) significantly reduced the proliferation and survival of OS cells by degrading BRD4. In addition, we found that GNE-987 markedly induced cell cycle arrest and apoptosis in OS cells. Further study indicated that VHL was critical for GNE-987 to exert its antitumor effect in OS cells. Consistent with in vitro results, GNE-987 administration significantly reduced tumor size in xenograft models with minimal toxicity, and partially degraded the BRD4 protein. KRT80 was identified through analysis of the RNA-seq and ChIP-seq data. U2OS HiC analysis suggested a higher frequency of chromatin interactions near the KRT80 binding site. The enrichment of H3K27ac modification at KRT80 was significantly reduced after GNE-987 treatment. KRT80 was identified as playing an important role in OS occurrence and development.

Conclusions This research revealed that GNE-987 selectively degraded BRD4 and disrupted the transcriptional regulation of oncogenes in OS. GNE-987 has the potential to affect KRT80 against OS.

Keywords OS, BRD4, SEs, PROTAC, KRT80

†Di Wu, Hongli Yin and Chun Yang contributed equally to this work.

*Correspondence:
Gen Li
ligen925@yeah.net
Jian Pan
panjian2008@163.com
[1]Institute of Pediatric Research, Children's Hospital of Soochow University, No.92 Zhongnan Street, SIP, Suzhou 215003, China

© The Author(s) 2024. **Open Access** This article is licensed under a Creative Commons Attribution-NonCommercial-NoDerivatives 4.0 International License, which permits any non-commercial use, sharing, distribution and reproduction in any medium or format, as long as you give appropriate credit to the original author(s) and the source, provide a link to the Creative Commons licence, and indicate if you modified the licensed material. You do not have permission under this licence to share adapted material derived from this article or parts of it.The images or other third party material in this article are included in the article's Creative Commons licence, unless indicated otherwise in a credit line to the material. If material is not included in the article's Creative Commons licence and your intended use is not permitted by statutory regulation or exceeds the permitted use, you will need to obtain permission directly from the copyright holder.To view a copy of this licence, visit http://creativecommons.org/licenses/by-nc-nd/4.0/.

Introduction

Osteosarcoma (OS) is one of the most common primary malignant bone tumors in children. OS develops from osteoblasts and usually occurs during rapid skeletal growth. The incidence of OS in the general population is 2–3 cases per million per year, and nearly 3/4 of patients are aged between 15 and 25 years [1, 2]. Patients with osteosarcoma have a low survival rate, with a 5-year overall survival of only 60–70%, dropping to approximately 20% when lung metastases develop [2]. In clinical practice, some children who suffer from osteosarcoma have high malignancy and early distant metastasis, and approximately 70% of the patients with osteosarcoma already have distant metastasis before diagnosis [3]. Although the therapeutic strategy has been improved in recent years, the prognosis of patients with lung metastasis is still disappointing, and the survival rate of most patients with lung metastasis is still poor even after effective treatment [4–7].

Tumor development is a complex and variable process, which results from uncontrolled regulation of gene function under the combined effect of genetic and epigenetic abnormalities [8]. Numerous studies have shown that epigenetic abnormalities play an essential role in tumorigenesis and development, and can regulate the transcription of relevant genes to contribute to tumorigenesis, metastasis, drug resistance, and recurrence [9, 10]. Chromatin remodeling is an important mechanism of epigenetic regulation that regulates gene expression and participates in the growth, proliferation, and differentiation of normal cells and the malignant transformation of cells. Acetylation modification is an important facet of histone chromatin remodeling. Acetylation loosens the binding of histones to chromatin, leading to the altered recruitment of transcriptional complexes, which in turn activates gene transcription. Aberrant histone epigenetic modifications may be important in controlling the expression of dysfunction-related genes in cells, especially in tumor cells.

BET proteins recruit transcriptional regulators to bind to histones through the bromodomain to exert transcriptional regulation, DNA damage and repair, and chromatin remodeling [11]. The BET family mainly consists of four isoforms, including BRD2, BRD3, BRD4, and BRDt, with different biological functions [12, 13]. Among them, BRD4 is the most extensively studied and essential member of the family, which contains two tandem structural domains BD1, and BD2, along with an ET structural domain [14]. Studies have shown that BRD4 is involved in mitotic chromosome remodeling and affects cell cycle regulation, while uncontrolled expression of BRD4 promotes the development of a variety of tumors, including hematological malignancies [15], colorectal cancer [16], prostate cancer [17], and breast cancer [18]. Because of its important role in regulating cell cycle progression, BRD4 has been identified as a target protein for novel targeted therapeutic agents for a wide range of malignant tumors [19–21].

Super-enhancers (SEs) are defined as ultra-long cis-acting elements with transcriptional enhancement activity of 8–20 kb in length, which can be enriched for a high density of key transcription factors and their cofactors. When compared to regular enhancers, SEs have a heightened transcriptional activation capacity that defines cellular identity and can drive the expression of key oncogenes in tumors [22, 23]. The clinical treatment of tumors can be significantly improved through the discovery and investigation of inhibitors targeting SEs, as tumor cells are exceptionally sensitive to targeted inhibition of SEs. The interaction of SE complexes is necessary for the activation of SEs, and researchers believe that designing inhibitors targeting SE complexes is the most effective approach. Currently, SE complex inhibitors used for cancer drug therapy mainly include inhibitors targeting the BRD family (JQ1, OTX-015, etc.), CDK7 inhibitors (SY-1365, THZ1, etc.) and other inhibitors (dinaciclib, trilaciclib, etc.) [24].

Among these inhibitors targeting the SE complex, BRD4 inhibitors are more widely used. BRD4 is an epigenetic factor that can localize to DNA by directly binding to acetylated histone lysine residues. It is then phosphorylated by recruiting positive transcription elongation factor b (p-TEFb), thereby activating RNA polymerase II (RNA-Pol II) to directly promote transcription initiation and elongation [25, 26]. BRD4 inhibitors specifically disrupt the binding activity of BRD4, one of the components of the SE complex, reducing SE-driven transcription of oncogenes and attenuating cancer cell proliferation [14]. Currently, small-molecule inhibitors targeting BRD4 include JQ1, iBET151, BMS-986,158, PLX-51,107, and ABBV-075. These inhibitors have demonstrated significant efficacy both in vivo and in vitro, with JQ1 being the earliest reported and most studied.

GNE-987 is a pan-BET inhibitor based on the von Hippel-Lindau tumor suppressor (VHL) that targets PROTAC, which binds to BET proteins (BRD2, BRD4, and BRD4) and facilitates their specific degradation via the ubiquitin/proteasome system [27, 28]. GNE-987 was shown to be a more potent BRD4 inhibitor in vitro compared to standard PROTACs MZ1, ARV-825, and JQ1 [9, 29]. No study has yet evaluated the role of GNE-987 in OS, so this study aimed to investigate the effects of GNE-987 on OS both in vitro and in vivo.

Materials and methods

Cell lines and cell culture

The human cell lines HOS,143B, U2OS, MG-63, and 293FT were purchased from Procell Life Science &

Technology and FuHeng Biology. 293T and U2OS cells (Procell, CL-0005; Procell, CL-0236) were maintained in Dulbecco's Modified Eagle's Medium (DMEM, BasalMedia). HOS,143B and MG-63 cells (FuHeng, FH0440; FuHeng, FH0438; Procell, CL-0157) were grown in Minimum Essential Medium alpha (MEM-α, BasalMedia). All the cell lines were tested for authentication using short tandem repeat fingerprinting. All cells were supplemented with 10% fetal bovine serum (FBS, Lonsera) and penicillin/streptomycin (Beyotime, 10 kU/mL). Cells were maintained in a humidified incubator with 5% CO2 at 37 ℃.

Immunohistochemistry (IHC) assay

IHC assays were performed based on microwave-enhanced avidin biotin staining as described below. Animal tumors or tissues were fixed in 4% paraformaldehyde and prepared as tumor tissue slides by paraffin embedding. Osteosarcoma tissue microarrays and tumor tissue slides were deparaffinized in xylene overnight at 65 °C and then hydrated using graded ethanol. The slides were boiled in 0.01 M citrate buffer for 5 min in a microwave oven and cooled at room temperature. Endogenous peroxidase activity was inhibited by incubating the slides in 3% H_2O_2 for 10 min at 37 °C. The slides were blocked with 3% BSA for 30 min at room temperature and then incubated with anti-BRD4 and anti-Ki-67 rabbit monoclonal antibodies overnight. The slides were rinsed in PBS and then co-incubated with the rabbit secondary antibody for 30 min at room temperature. DAB staining was performed for 5 min at room temperature and then rinsed with distilled water and analyzed by light microscopy after counterstaining with hematoxylin. Cells in the sections were scored according to whether they were stained or not and the degree of staining: no staining was scored as 0, light brown was scored as 1, medium brown was scored as 2, and dark brown was scored as 3. The percentage of positive staining in the sections was scored as follows: <5% as 0, 5-25% as 1, 25-50% as 2, and >50% as 3. The two scores were multiplied to obtain a final score: 0–4 was categorized as low expression, and a final score above 4 was categorized as high expression.

Cell viability assay

Cell viability was assessed with Cell Counting Kit 8 (CCK-8, Dojindo, Japan) according to the manufacturer's protocol. OS cell lines [U2OS, MG-63,HOS and 143B] 8×10^3 per 150 μL were seeded into 96-well plates at 37℃ with 5% CO_2. After cell attachment, the cells were treated with a gradient concentration (0.625-160 nM) of GNE-987 (MedChemExpress, USA). After 48 h,10 μL CCK-8 was added and incubated for 2 h at 37 ℃. HOS cells with KRT80 knockdown were seeded into 96-well plates. At 0, 24, 48,72, and 96 h after seeding, 10 μL CCK-8 was added and incubated for 2 h at 37 ℃. The absorbance of the solution was measured at 450 nm. IC50 values and relative survival rates of OS cells treated with GNE-987 were calculated using GraphPad Prism (9.5.0).

Colony formation assay

OS cells in the exponential phase were taken and inoculated in six-well plates with a density of 1000 cells per well, gently blown to disperse the cells evenly, and cultured in a cell incubator for 7–12 days. When clones were visible, the supernatant was discarded, and the cells were washed with PBS, and fixed with methanol for 10 min, then stained with Giemsa staining solution for 10 min at room temperature, rinsed twice with PBS, and dried at room temperature. The number of cell clones was read using ImageJ(ImageJ, RRID: SCR_003070).

Cell cycle assay

HOS and 143B were seeded into 6-well plates at 37℃ with 5% CO_2. After cell attachment, the cells were treated with DMSO and GNE-987. The collected OS cells were centrifuged at 300 g for 5 min, the supernatant was discarded and cold PBS was added to resuspend cells at 300 g for 5 min, and the supernatant was discarded. Add 1 mL of precooled 70% ethanol, gently blow and mix, and fix at 4 °C overnight. Cells were collected at 600 g centrifugation for 5 min, 1 mL of cold PBS was added to resuspended cells, and RNase and PI were added to incubate for 30 min at room temperature without light, followed by placing the samples in a flow cytometry for sample detection.

Cell apoptosis assay

HOS and 143B were seeded into 6-well plates at 37℃ with 5% CO_2. After cell attachment, the cells were treated with DMSO and GNE-987. The OS cell culture supernatant and digested cells were placed in the same centrifuge tube and centrifuged at 300 g for 5 min. The supernatant was removed and PBS was added to resuspend the cells, after centrifugation again, the cells were resuspended by adding a certain amount of binding buffer to make the concentration of the cells ~ 1×10^6/mL. 100 μL of cell suspension was aspirated, and 5 μL of Annexin V-FITC and 5 μL of PI were added to the cell suspension and gently mixed after incubation for 20 min at room temperature without light. Then the samples were placed in a flow cytometer for sample detection.

Western blotting

Total OS cell proteins were extracted using RIPA lysis buffer (Beyotime, China) containing protease inhibitors (Roche, Switzerland). Western blot was performed as described previously [29]. The membrane was incubated overnight at 4 ℃ with primary antibodies against:

BRD4(Cell Signaling Technology Cat# 13440, RRID: AB_2687578), Ki67(Abcam Cat# ab16667, RRID: AB_302459), BRD2(Cell Signaling Technology Cat# 5848, RRID: AB_10835146), BRD3(Proteintech Cat# 11859-1-AP, RRID: AB_2065902), PARP(Cell Signaling Technology Cat# 9542, RRID: AB_2160739), RUNX2(Cell Signaling Technology Cat# 12556, RRID: AB_2732805), Cyclin B1(Cell Signaling Technology Cat# 12231, RRID: AB_2783553), VHL(Cell Signaling Technology Cat# 68547, RRID: AB_2716279), KRT80(Proteintech Cat# 16835-1-AP, RRID: AB_1851273) and GAPDH(Cell Signaling Technology Cat# 5174, RRID: AB_10622025). The following day, the membranes were incubated with goat anti-mouse HRP-conjugated secondary antibody (115035-003, Jackson ImmunoResearch Laboratories) or goat anti-rabbit HRP-conjugated secondary antibody (111035-003, Jackson ImmunoResearch Laboratories) for 1.5 h. Chemiluminescence was determined using the Pierce™ ECL Western detection system (Thermo Scientific, USA).

RT-qPCR

Total RNA from OS cells was extracted by trizol. The obtained RNA was then reverse-transcribed into cDNA by HiScript III RT SuperMix according to the manufacturer's protocol. The cDNA was added to a mixture containing primers and SYBR Green, then placed in a LightCycler 480 Real-Time System for RT-qPCR analysis. Human GAPDH was used as an endogenous control, and the $2^{-\Delta\Delta CT}$ method was applied to calculate the relative expression of mRNA. The primer sequences were as follows: GAPDH, 5'-CTGGGCTACACTGAGCACC-3'(Forward) and 5'-AAGTGGTCGTTGAGGGCAATG-3'(Reverse); KRT80, 5'-CCTCCCTAATTGGCAAGGTG-3'(Forward) and 5'-AGATGCCCGAGGTCGAAGAT-3'(Reverse); other primers are available in Supplementary information (Supplementary Table 1).

Xenograft tumor and GNE-987 treatment in nude mice

For the in vivo tumor model, 2×10^6 HOS cells were subcutaneously injected into 10 BALB/c nude mice (two groups of five). One week after transplantation, tumor mice were injected with 100 μL of 0.2 mg/kg GNE-987 or the same dose of the vehicle as the test group every two days, and the size of tumors was measured every three days. After 18 days, the mice were humanely euthanized, and the tumors were dissected out completely with a scalpel. The tumors were weighed and fixed with 4% paraformaldehyde for immunohistochemical and HE staining histological examination.

Hematoxylin-eosin (HE) staining

After routine deparaffination, the sections were stained with hematoxylin stain for about 5 min and then rinsed clean with deionized water. The sections were soaked in 1% ethanol hydrochloric acid solution for 10 s at room temperature and then placed in 0.6% ammonia solution and rinsed clean using deionized water. They were stained with eosin stain for about 3 min and rinsed clean using deionized water. Alcohol, dimethylbenzene, and neutral gum were separately and sequentially used for dehydration, hyalinization, and sealing.

ChIP-seq

Approximately 3×10^7 OS cells were collected and cross-linked with 1% paraformaldehyde for 10 min at room temperature, followed by the addition of an equal volume of 0.25 M glycine to terminate cross-linking. After centrifugation at 200 g for 5 min, the supernatant was discarded, and the cells were resuspended in Lysis Buffer supplemented with protease inhibitors and placed on ice for 5 min. The cell membrane was then broken by repeated pipetting with an insulin needle, and the supernatant was discarded after centrifugation at 13,000 g for 5 min (this step was repeated). Resuspend the pellet with shearing buffer and transfer it to an ultrasonic tube, and use a sonicator to sonicate for 5 min to shear the genomic DNA into fragments with a length of 300–800 bp. The sonicated liquid was centrifuged at 13,000 g for 10 min, the supernatant was aspirated and divided into two parts, 20 μL of which was used as input of the sample, and the remaining sample was incubated with H3K27ac antibody overnight at 4℃ for pre-binding. Dynabeads Protein G beads were added to the samples and the incubation was continued for 4 h at 4℃. The antibody-chromatin on the beads was washed 6 times with lysis buffer followed by 2 times with TE buffer. After bead washing, EB buffer was added to each sample to separate the antibody and chromatin from the Protein G beads, followed by 5 M NaCl incubation at 65℃ overnight to complete de-crosslinking. RNase (#7013, CST) was added and incubated at 37 °C for 30 min to remove contaminating RNAs. 20 mg/mL Proteinase K (AM2546, Invitrogen), 0.5 M EDTA (pH 8.0), and 1 M Tris HCl (pH 8.0) were added and incubated at 45 °C for 1 h to remove proteins. The obtained DNA fragments were purified with a DNA purification kit and subjected to agarose gel electrophoresis to detect the length of the DNA fragments. The samples were finally sent to BGI Genomics and the raw data obtained were submitted to the Gene Expression Omnibus (GEO, RRID: SCR_005012) database (GSE243673).

Hi-C interactions

The Hi-C data of osteosarcoma cell line U2OS was downloaded from the GEO database (GSE 164777) and processed using Hi-C-pro (v.3.1.0).

RNA-seq and data analysis

RNA-seq was implemented according to the protocols provided by Novogene (Beijing, China). The total RNA of OS was extracted by trizol and sent to Novogene, which completed the purification, quality control, library construction, and sequencing of RNA. RNA-seq raw data have been uploaded to the Gene Expression Omnibus (Geo, RRID: SCR_005012) database (GSE243673). The Bioconductor (RRID: SCR_006442) DESeq2 (RRID: SCR_000154) package 1.32.0 was used to identify differentially expressed genes. Gene set enrichment analysis (GSEA, RRID: SCR_003199) was performed using the clusterProfiler (RRID: SCR_016884) package 4.0.5 inR 4.1.1.

Vector construction and viral infection

Packaging plasmid (pMD2.G, RRID: Addgene_12259; psPAX2, RRID: Addgene_12260) was provided by Addgene (Massachusetts, USA). Multiple shRNA sequences targeting VHL, KRT80 and negative control in PLKO.1 lentiviral vector were designed and constructed by General Biol (Anhui, China). The targeting sequence for VHL was 5′-CCGGGCTCAACTTCGACGGCGAGCCCTCGAGGGCTCGCCGTCGAAGTTGAGCTTTTTGAATT-3′; the targeting sequence for KRT80#1 was 5′- CCGGGCATCTCTATGAGGAATATCACTCGAGTGATATTCCTCATAGAGA.

TGCTTTTTGAATT-3′; the targeting sequence for KRT80#2 was 5′- CCGGGCGAGATCGCGG.

ATCTCAATGCTCGAGCATTGAGATCCGCGATCTCGCTTTTTGAATT-3′; the targeting sequence for KRT80#3 was 5′- CCGGGACATGGAGTTCACCTTTGTTCTCGAGAACAAAG.

GTGAACTCCATGTCTTTTTGAATT-3′.

Overexpression sequences targeting VHL in the PLVX-Flag lentiviral vector and negative control (PLVX-NC) were purchased from General Biol. The target plasmid and the packaging plasmid were transfected into 293T cells using PEI, and after 48 h the medium supernatant was collected and the virus was concentrated using PEG8000. After 16–24 h of lentivirus infection of the cells with lentivirus, the medium was changed to a complete medium containing 1.5 μg/mL puromycin and puromycin was selected to establish stably transfected OS cells.

Statistical analysis

Statistical analysis was performed using GraphPad Prism (RRID: SCR_002798) and the R language, and the difference between the two groups was performed using a double-tailed paired Student's T-test. Differences between groups were compared using one-way analysis of variance. A P value less than 0.05 was considered statistically significant ($^{*}p<0.05$, $^{**}p<0.01$, $^{***}p<0.001$,). The mean ± standard deviation (SD) is shown.

Results

Tumor progression is associated with high BRD4 expression in OS

To preliminarily determine the clinical significance of BRD4 in osteosarcoma, we examined BRD4 expression in tissue microarrays generated from osteosarcoma patient samples. BRD4 expression was detected using immunohistochemistry (IHC) on samples from 20 patients with OS and 5 corresponding paracancerous normal tissues. The results showed that nuclear staining of BRD4 was more pronounced in osteosarcoma compared to paracancerous tissues, indicating that BRD4 protein expression was elevated in OS tissues (Fig. 1A). The above results suggested an association between BRD4 and OS, revealing that BRD4 may be an important therapeutic target for OS.

Previous studies showed that JQ1 and MZ1 exhibited valid antitumor effects in osteosarcoma and various other tumors by targeting BRD4. Next, we compared the ability of GNE-987 with JQ1 and MZ1 to inhibit cell viability by examining the IC50 of HOS and 143B cells after drug treatment. The same number of cells were treated with increasing concentrations of GNE-987, JQ1, and MZ1 for 48 h, and cell viability was subsequently assessed using CCK-8 assay. Dose-dependent inhibition of cell growth was observed in all three drug-treated groups, and the half-inhibitory concentration of GNE-987 was much lower than that of the other two drugs (Fig. 1B). In conclusion, GNE-987 inhibited the proliferation of HOS and 143B cells at lower concentrations, indicating that this novel PROTAC bromodomain inhibitor has a superior inhibitory effect on HOS and 143B cells.

GNE-987 disrupts the biological functions of OS cells

To further evaluate the effect of the BRD4 inhibitor on OS cell proliferation and viability, we initially examined the cytotoxicity of GNE-987 on different OS cells. We treated four OS cell lines with a gradient concentration of GNE-987 and measured cell viability using CCK-8 at 48 h. The CCK-8 results indicated that GNE-987 exerted a significant inhibitory effect on all four OS cell lines (U2OS IC50, 6.84 nM; HOS IC50, 2.46 nM; MG-63 IC50, 5.78 nM;143B IC50, 7.71 nM) (Fig. 2A-B). We have detected that BET family members are commonly expressed in OS cell lines (Fig. 2C). Further observation revealed that there were significant changes in cell morphology in the drug-treated group, as evidenced by cell shrinking and floating (Fig. 2D). Subsequently, we evaluated the effect of GNE-987 on the malignant proliferation ability of OS cells by colony formation assay, and the results showed that GNE-987 inhibited the colony formation of OS cells in a dose-dependent manner when compared to the control group (Fig. 2E-F). Overall, these results indicated that GNE-987 exhibits potent

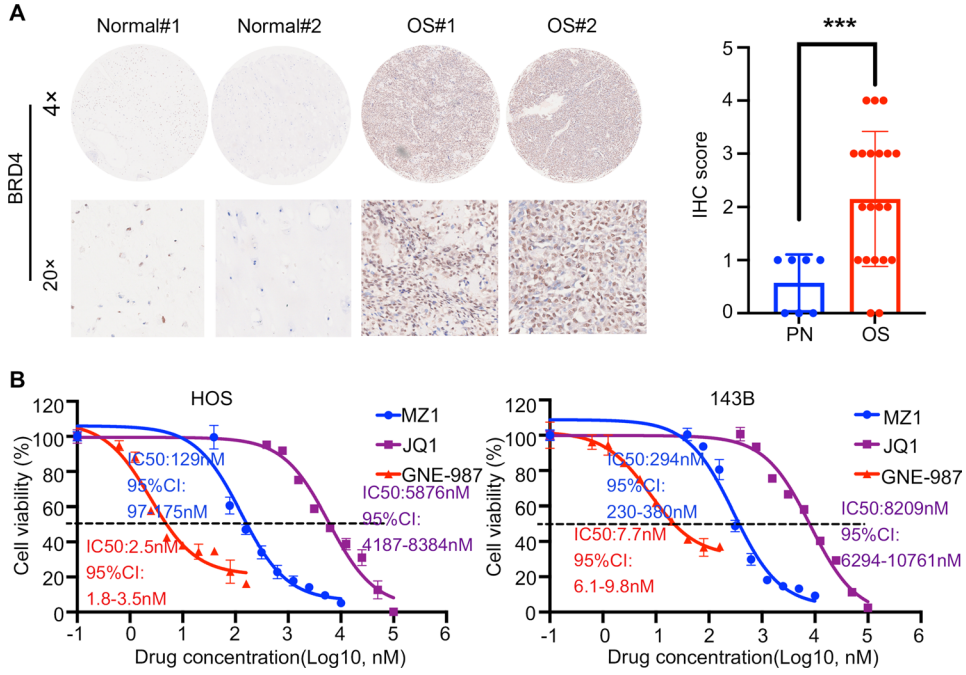

Fig. 1 Tumor progression is associated with high BRD4 expression in OS. (**A**). The typical image of BRD4 protein IHC staining on a tissue microarray consisting of 20 OS tissues and 5 normal paraneoplastic tissues. Histochemical scores were evaluated based on the intensity of BRD4 staining. Normal: paraneoplastic normal tissue; OS: osteosarcoma tissue. ***$p<0.0001$. (**B**). Half-inhibitory concentrations of three BRD4 inhibitors (GNE-987, JQ1, MZ1) in HOS and 143B cells were detected by CCK-8. Data were represented as the mean ± SD

cytotoxicity and proliferation inhibition of OS cell lines in vitro in a dose-dependent manner.

BRD4 blocks the cell cycle and induces apoptosis in OS cells

Previously, it was reported that BRD4 regulates DNA replication and gene transcription by binding to acetylated histones and non-histones, thereby affecting the cell cycle. As we know, GNE-987 acts as a direct PROTAC bromodomain inhibitor targeting BRD4. Therefore, we evaluated the effect of GNE-987 treatment on the OS cell cycle by flow cytometry. Treatment with GNE-987 resulted in G2/M arrest of OS cell lines compared to control groups using Modfit analysis (Fig. 3A). Cyclin B1, one of the cell cycle regulators, was also downregulated after GNE-987 treatment in a dose-dependent manner (Fig. 3B). In order to investigate the effect of GNE-987 on the proliferation of OS cells, we used Annexin V-FITC/PI staining to evaluate cell apoptosis and detected changes in cell apoptosis using flow cytometry. The CCK-8 results showed that the osteosarcoma cell lines all underwent GNE-987 dose-dependent apoptosis (Fig. 3C-D), and PARP was cleaved to different degrees after treatment with GNE-987 (Fig. 3B). The above results suggested that GNE-987 can inhibit the proliferation of OS cells by degrading BRD4 to regulate the cell cycle and induce apoptosis.

GNE-987 induces the degradation of BET protein and RUNX2

PROTAC acts as a small molecule inhibitor designed to target and degrade specific proteins. We used western blotting to detect changes in BET protein levels after treatment with GNE-987. Our results showed that GNE-987 degraded BET proteins in four OS cell lines in a concentration-dependent manner (Fig. 4A). We also examined the protein level of RUNX2, which is closely related to osteosarcoma, and showed that the protein level of RUNX2 was significantly down-regulated by GNE-987 treatment (Fig. 4A). The above results indicated that GNE-987 could target and degrade the BET proteins while also downregulating the expression of OS-associated transcription RUNX2 in OS cell lines.

VHL modulates OS cell sensitivity to GNE-987

Previous studies showed that binding of the essential role of the VHL substrate recognition subunit in mediating the degradation of BET family proteins induced by GNE-987 (Fig. 5A); therefore, we examined the sensitivity of HOS cells to GNE-987 after overexpression or knockdown of VHL. CCK-8 experiments demonstrated that overexpression of VHL increased the sensitivity of HOS cells to GNE-987 (Fig. 5B-C). Conversely, the downregulation of VHL increased the survival of HOS cells when treated with the same concentration of GNE-987 (Fig. 5B-C). The transformation of BET proteins is

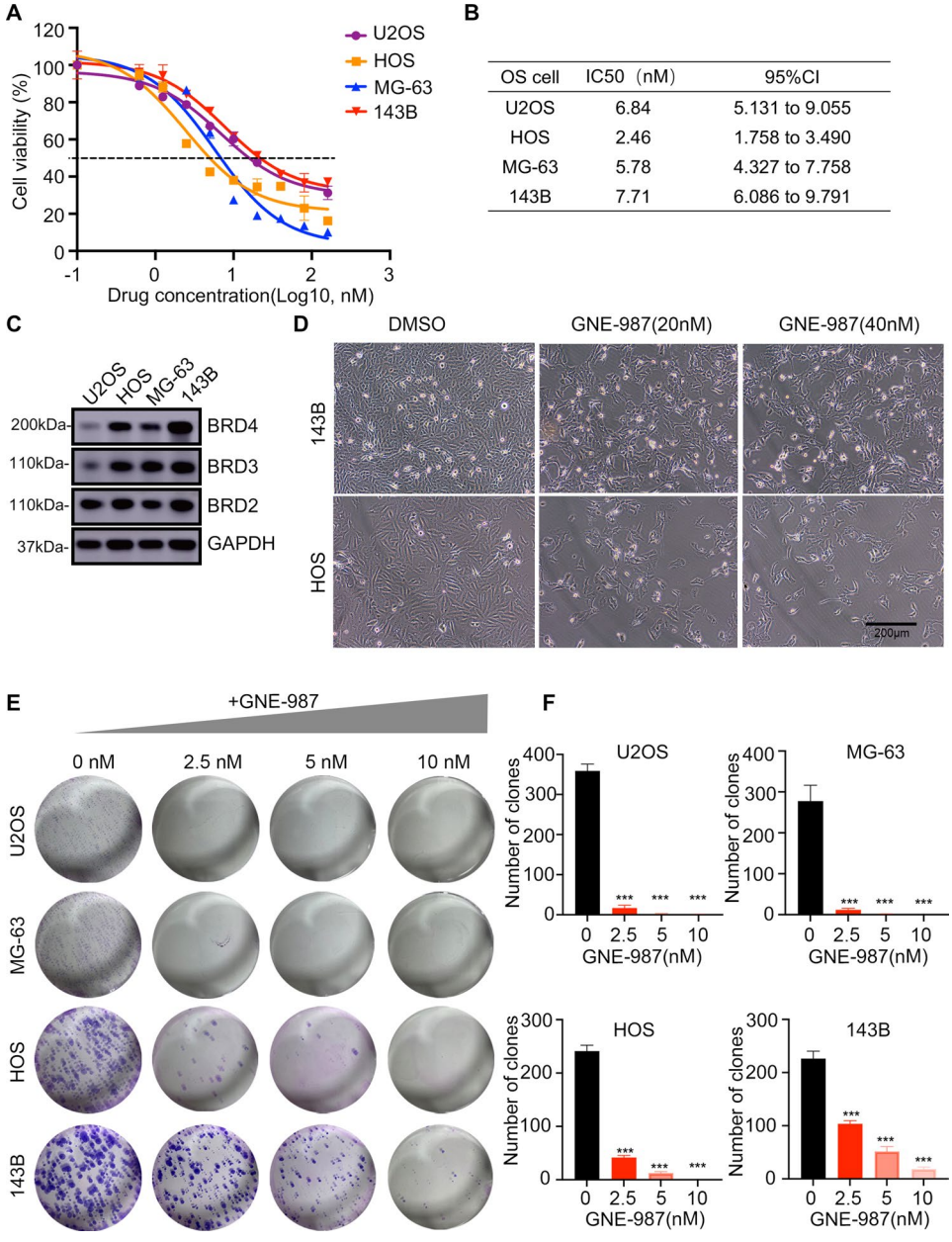

OS cell	IC50 (nM)	95%CI
U2OS	6.84	5.131 to 9.055
HOS	2.46	1.758 to 3.490
MG-63	5.78	4.327 to 7.758
143B	7.71	6.086 to 9.791

Fig. 2 GNE-987 disrupts the biological functions of OS cells. (**A**). Half-inhibitory concentrations of GNE-987 in four OS cell lines (U2OS, HOS, MG-63, 143B) were detected by CCK-8. (**B**). IC50 value of GNE-987 in four OS cell lines. (**C**). BET family protein levels in OS were evaluated by Western blotting. (**D**). Microscopic bright-field photographs of HOS as well as 143B cells after treatment with DMSO and different concentrations of GNE-987 for 24 h. (**E**, **F**). The colony formation assay was performed to assess the clonal formation ability of OS cells. ***$p<0.0001$. Data were represented as the mean ± SD

dependent on ubiquitin degradation and other inhibitors of the PROTAC bromodomain of BET proteins can down-regulate their expression through this mechanism. Therefore, we subjected the cells to treatment with the proteasome inhibitor MG132 and observed the ubiquitin-dependent degradation of BET proteins induced by GNE-987 (Fig. 5D). These results suggested that VHL plays a crucial role in the antitumor effects exerted by GNE-987 in OS cells.

GNE-987 shows anti-tumor activity in the xenograft model of osteosarcoma

The experimental results revealed the significant anti-osteosarcoma effect of GNE-987 in vitro. To further investigate the anti-tumor efficacy of GNE-987 in vivo, we constructed a subcutaneous loaded-tumor model of osteosarcoma by subcutaneous inoculation of HOS cells into the axilla of nude mice. Once the tumors reached a certain size, one group of mice with loaded tumors was given intraperitoneal injections of 0.2 mg/kg GNE-987

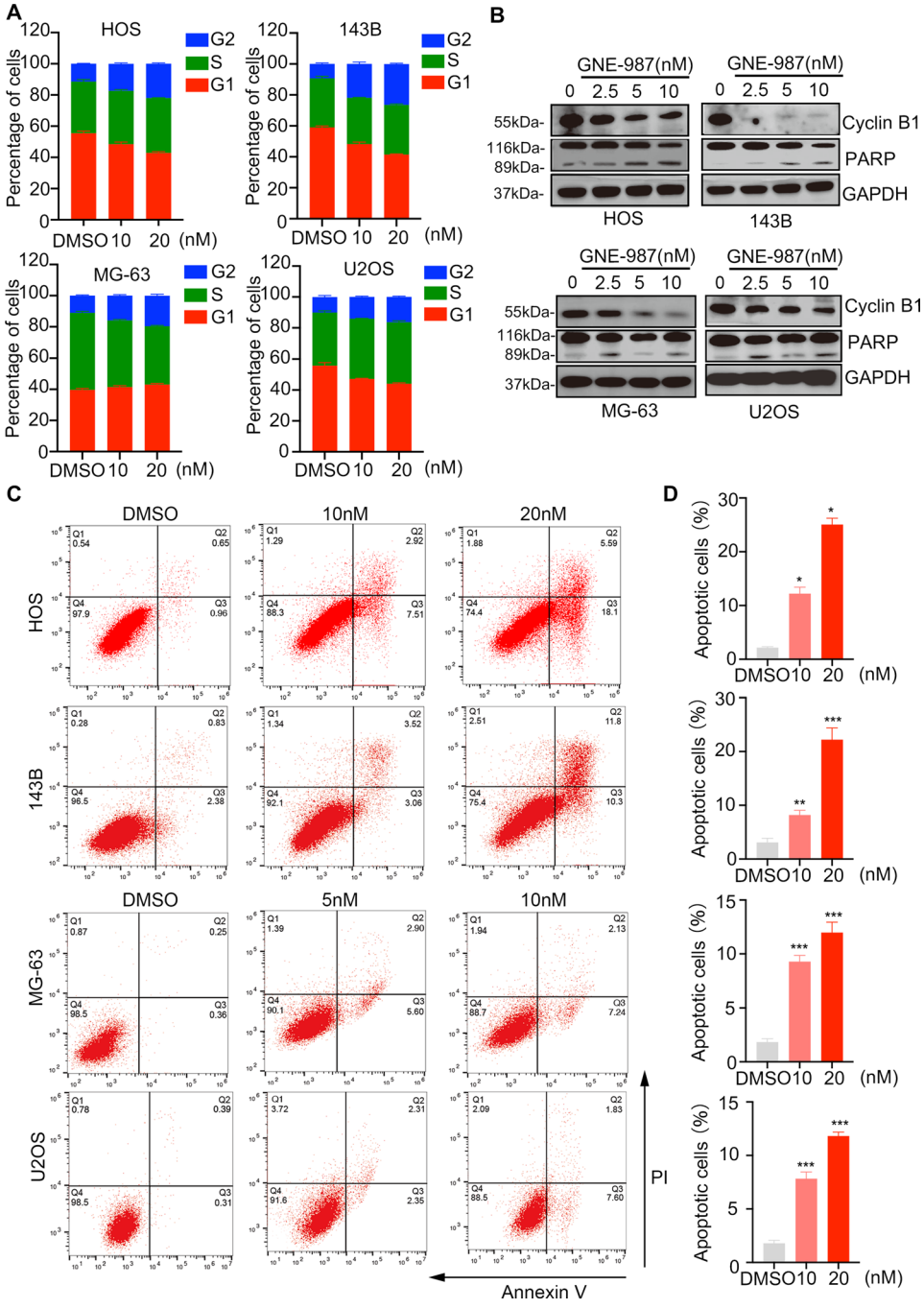

Fig. 3 BRD4 blocks the cell cycle and induces apoptosis in OS cells. (**A**). OS cells were collected after treatment with GNE-987 for 24 h and analyzed for cell cycle by flow cytometry. (**B**) The protein levels of cyclin B1 and cleaved PARP in the OS cell treated with DMSO and GNE-987 were assessed using Western blotting. (**C**, **D**). Cell apoptosis was detected in the OS cell treated with DMSO and GNE-987 by performing Annexin V/PI staining and flow cytometry. *$p<0.05$, **$p<0.01$, ***$p<0.001$. Data were represented as the mean ± SD

every two days, and the other group was injected with the same volume of drug solvent (5% Kolliphor) as the control group (Fig. 6A-B). Tumor size in the mice was measured every three days after the injection of the drug, and on the 18th day, the mice were humanely euthanized, the tumors and the surrounding adherent tissues were stripped, and the tumors were weighed (Fig. 3C-F). Our results showed that tumor mass and volume were significantly reduced in the GNE-987-treated group compared with the control group. Importantly, this treatment had minimal impact on the body weights of the mice (Fig. 6B), and there was no significant toxic response observed in the internal organs of the mice (Fig. 6G). The results of immunohistochemistry also showed that

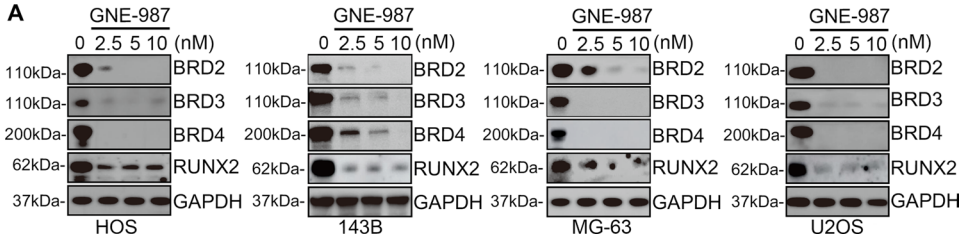

Fig. 4 GNE-987 induces the degradation of BET protein and RUNX2. (**A**). Western blotting analysis of BET protein and RUNX2 expression in OS cells after treatment with DMSO or increasing concentrations of GNE-987

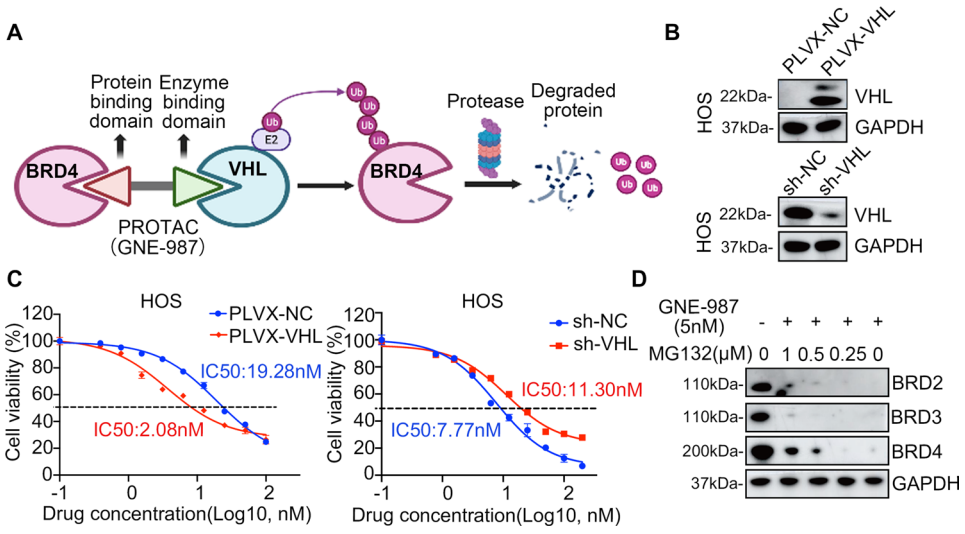

Fig. 5 VHL modulates OS cell sensitivity to GNE-987. (**A**). Diagram of the mechanism by which GNE-987 targets BRD4 for degradation: GNE-987 binds BRD4 and VHL E3 ubiquitin ligase and mediates the transfer of the E2 enzyme to the target protein BRD4. (**B**). Western blotting analysis of VHL expression in HOS cells (PLVX-NC/VHL; sh-NC/VHL). (**C**). The sensitivity of HOS cells (PLVX-NC/VHL; sh-NC/VHL) to GNE-987 was analyzed. (**D**). HOS cells were treated with the proteasome inhibitor MG132 and observed the ubiquitin-dependence of the degradation of BET proteins induced by GNE-987

GNE-987 treatment significantly reduced the expression levels of BRD4 and Ki-67 in the tumors (Fig. 6H-I). Overall, these results suggest that GNE-987 also exhibits potent anti-tumor properties in vivo.

Mechanism of anti-tumor effects of GNE-987 in OS

To investigate the potential mechanism by which GNE-987 inhibited the progression of osteosarcoma, we collected GNE-987-treated HOS cells for RNA-seq to analyze the differences in transcript levels and further screen for differentially expressed genes. After 24 h of 10 nM GNE-987 treatment, 5306 genes were down-regulated and 4368 genes were up-regulated in HOS cells by RNA-seq analysis (Fig. 7A, Supplementary Table S2). To further clarify the role of GNE-987 in gene regulation, we applied Hallmark pathway enrichment analysis to reveal the functions of differentially expressed genes. The results showed that the genes regulated by GNE-987 were closely related to the pathways related to tumor progression, such as "HALLMARK_G2M_CHECKPOINT" and "HALLMARK_APOPTOSIS", which had no significant correlation with "HALLMARK_MYC_TARGET_V2 (Fig. 7B)".

BRD4 inhibitors are known to disrupt the interaction of SEs with the complex, so GNE-987 can block the transcriptional activation of oncogenes dependent on SEs. Based on previous studies, we performed high-throughput sequencing by ChIP-seq to identify the H3K27ac region and screened for SE-related genes that were changed in OS after GNE-987 treatment. Our analysis revealed that the number of SE-regulated genes decreased after GNE-987 treatment (Fig. 7C, Supplementary Table S3). Further integration of RNA-seq and ChIP-seq results revealed 76 overlapping genes (Fig. 7D), suggesting that those genes were down-regulated by GNE-987 treatment while being regulated by the corresponding SE, which in turn affected the OS process. Many of the 76 genes have been identified as SE-associated genes (Fig. 7D), such as ZNF217 [30], among which LIF, RUNX2, and EGFR are transcription factors that play important roles in osteosarcoma survival [31–33]. In contrast, the oncogenic role of genes like KRT80 in osteosarcoma has not been reported previously. To confirm the

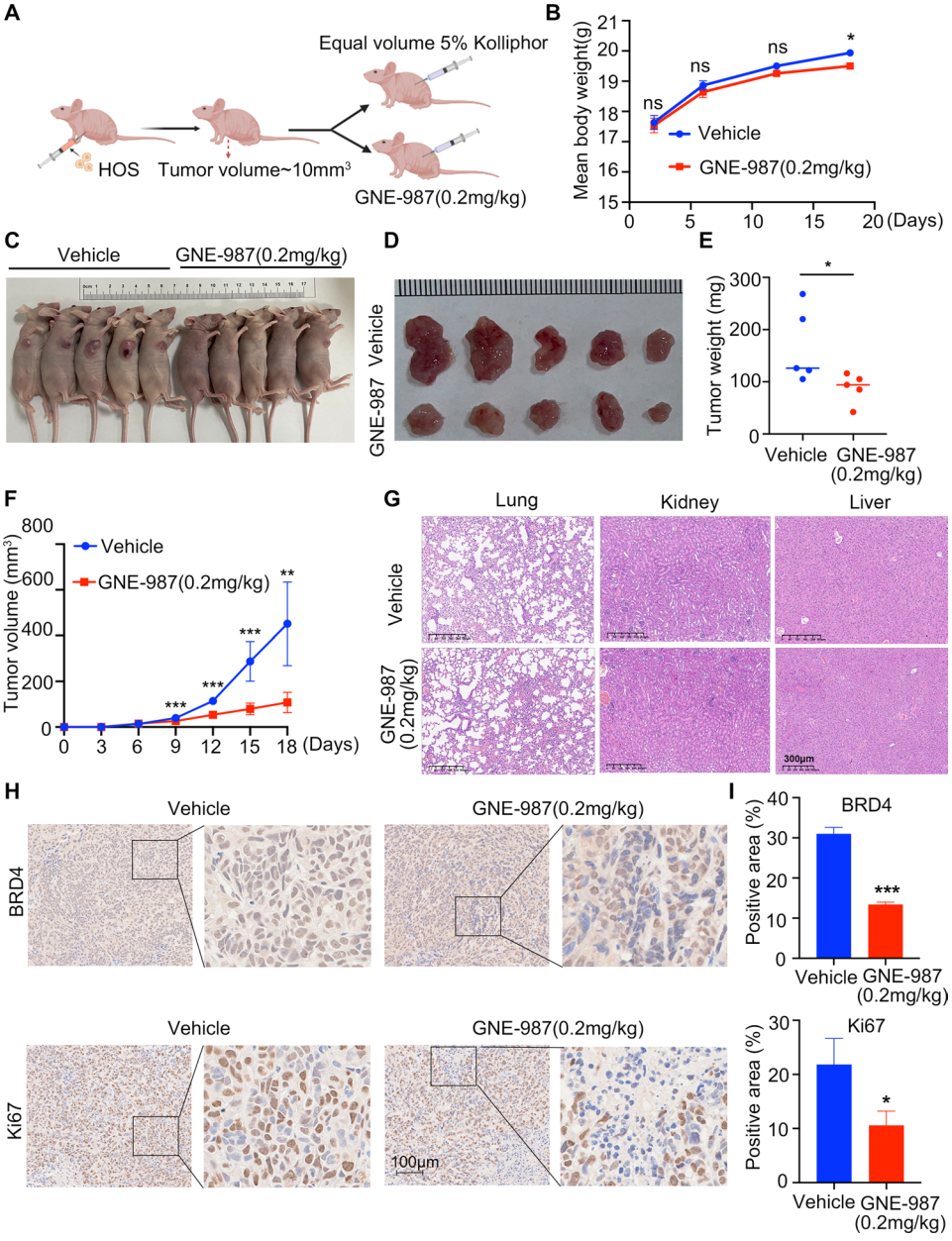

Fig. 6 GNE-987 shows anti-tumor activity in the xenograft model of osteosarcoma. (**A**). A subcutaneous loaded-tumor model of osteosarcoma was constructed by subcutaneous inoculation of HOS cells into the axilla of nude mice. Mice were treated with drug solvent (5% Kolliphor) or GNE-987 every two days once the tumor volume reached approximately 10 mm3. (**B**). Mice were weighed every five days. (**C**-**E**). On the 18th day, the mice were euthanized, and the tumors and the surrounding adherent tissues were stripped. (**F**). The size of the tumors of the mice was measured every three days after the injection of the drug. (**G**). Comparison of HE staining of visceral tissues from mice treated with control and GNE-987. (**H**, **I**). Representative images of IHC staining with antibodies in tumors isolated from two groups of mice. *$p<0.05$, **$p<0.01$, ***$p<0.001$. Data were represented as the mean ± SD

gene changes after GNE-987 treatment, we quantified the expression of SE-related genes after DMSO or GNE-987 treatment by RT-qPCR, and the assay results verified the down-regulation of the mRNA levels of these SE-related genes in RNA-seq (Fig. 7E). The above results indicated that downregulation of BRD4 expression weakened the regulatory effect of SE on related genes in OS, and GNE-987 inhibited osteosarcoma progression by selectively targeting BRD4 to regulate SE-related genes.

KRT80 is a novel target of GNE-987 in OS

To further identify and validate the SEs of OS, we performed the H3K27ac ChIP-seq on 4 osteosarcoma cell lines. We downloaded the H3K27ac ChIP-seq of 4 osteosarcoma samples and 1 osteoblast cell line, and

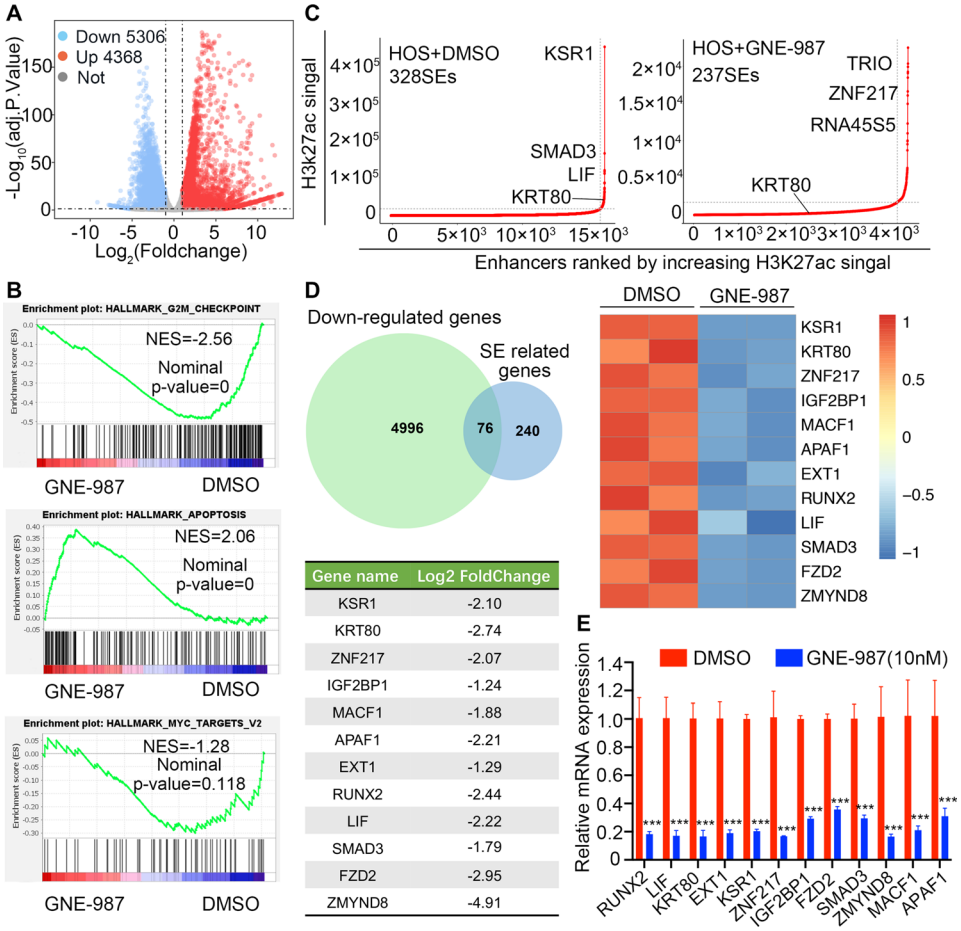

Gene name	Log2 FoldChange
KSR1	-2.10
KRT80	-2.74
ZNF217	-2.07
IGF2BP1	-1.24
MACF1	-1.88
APAF1	-2.21
EXT1	-1.29
RUNX2	-2.44
LIF	-2.22
SMAD3	-1.79
FZD2	-2.95
ZMYND8	-4.91

Fig. 7 Mechanism of anti-tumor effects of GNE-987 in OS. (**A**). Volcano plot of gene expression differences between GNE-987 and DMSO-treated HOS cells. Blue and red dots mark all transcripts with statistically significant expression down/up-regulation (log2FoldChange < – 1.0 or > 1, $p < 0.05$). (**B**). Enrichment analysis of differentially expressed genes using the GSEA pathway database to screen for pathways associated with regulation by the GNE-987. (**C**). The enhancers treated with DMSO and GNE-987 in HOS were ranked according to the signal intensity of H3K27ac, and the number of SEs in each group is indicated in the figure. (**D**). Venn diagram of 76 overlapping genes between RNA-seq down-regulated genes and SE-related genes obtained by analyzing ChIP-seq. The heatmap shows the relative expression levels of the representative genes among the 76 genes, and the table shows the fold change of the representative genes. (**E**). RT-qPCR analysis of representative genes. ***$p<0.001$. Data were represented as the mean ± SD

the H3K4me1 results of 1 osteosarcoma sample from the Cistrome Data Browser. The results showed that in 4 osteosarcoma samples and 4 OS cell lines, there was a significant enrichment of H3K27ac at the KRT80 location, suggesting the presence of a SE that regulates KRT80 (Fig. 8A). However, there was no significant enrichment of H3K27ac in normal osteoblasts, suggesting that KRT80 was specifically activated in OS cells (Fig. 8A). U2OS HiC analyses showed a high frequency of chromatin interactions in the vicinity of the KRT80 binding site linking the promoter to the super-enhancer (Fig. 8A). The enrichment of H3K27ac modification at KRT80 was significantly reduced after GNE-987 treatment (Fig. 8B). KRT80 was downregulated after GNE-987 treatment in a dose-dependent manner (Fig. 8C). Similarly, the KRT80 protein was significantly downregulated after treatment with GNE-987 in the xenograft model of osteosarcoma(Fig. 8D). The above results suggested that GNE-987 treatment invaded the super-enhancer, decreased the enrichment of H3K27ac at KRT80, and may alter the chromatin interactions between the promoter and enhancer.

To verify the oncogenic role of KRT80 in OS, we down-regulated the expression of KRT80 in HOS cells by specific shRNA and verified by RT-qPCR and western blotting (Fig. 8E-F). The downregulation of KRT80 expression led to a significant decrease in the proliferation of HOS cells (Fig. 8G). Consistent results were obtained in colony formation experiments, the results of clone formation experiments showed that the colony formation ability of HOS cells was significantly decreased after KRT80 knockdown (Fig. 8H-I). Taken together, the results indicated that KRT80 promotes the survival and growth of OS cells, which is in line with the prediction of our bioinformatics analysis and is also expected to

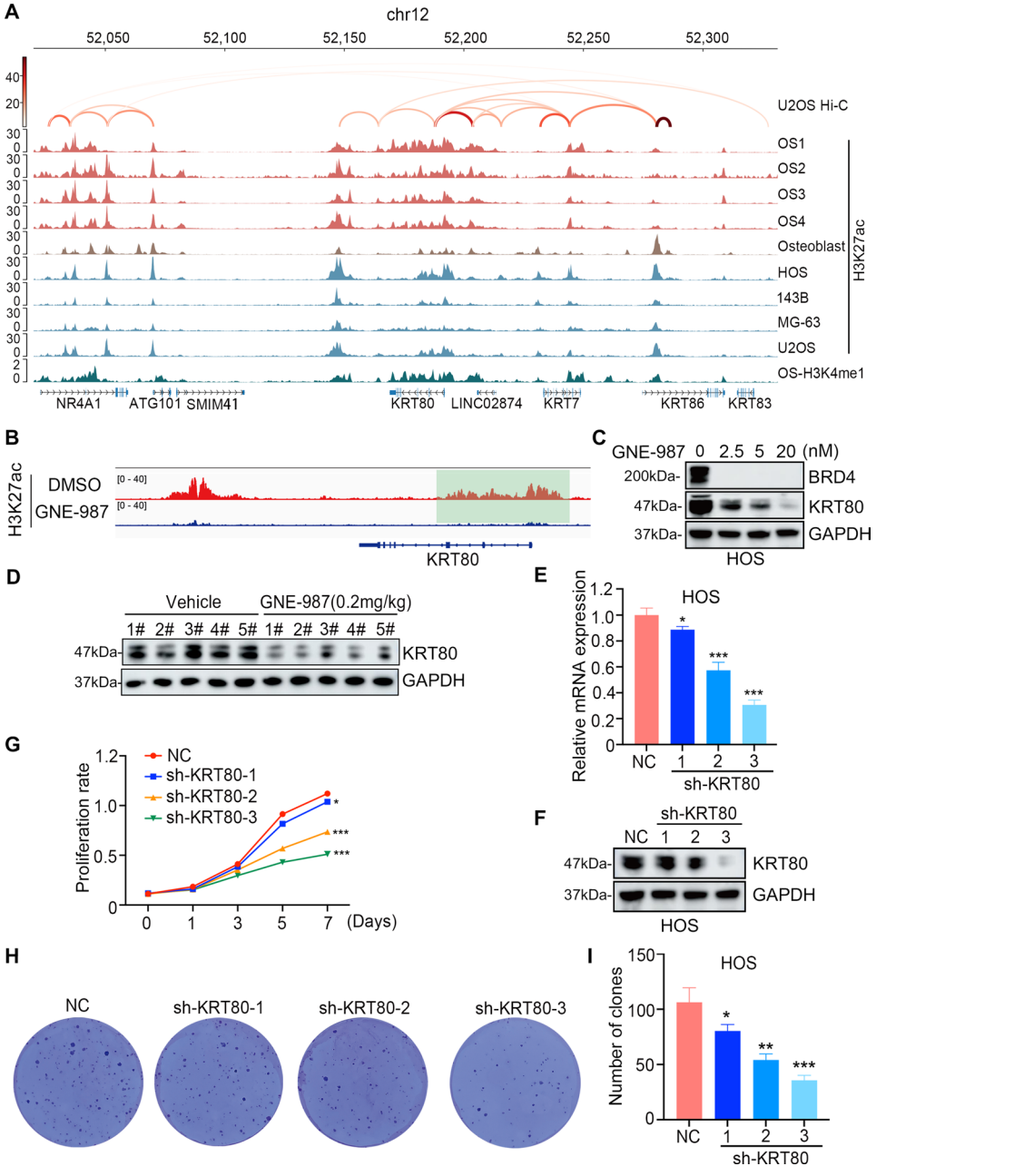

Fig. 8 KRT80 is a novel target of GNE-987 in OS. (**A**). IGV plot showing KRT80 ChIP-seq and Hi-c profiles in OS motifs. ChIP-seq gene tracks represent H3K27ac enrichment signals in OS clinical samples (red and green), normal osteoblastic tissue (brown), and OS cell lines (blue). (**B**). IGV plot showing the enrichment of H3K27ac modification at KRT80(DMSO-treated group: red; GNE-987-treated group: blue). (**C**). KRT80 protein expression was quantified after GNE-987 treatment by Western blotting in HOS cells. (**D**). KRT80 protein expression was quantified after GNE-987 treatment by Western blotting in the xenograft model of osteosarcoma. (**E**, **F**). HOS cells were transfected with sh-NC, sh-KRT80-1, sh-KRT80-2, or sh-KRT80-3, respectively, and positive cells were obtained after screening with puromycin for 5 days. The expression of KRT80 was detected by qRT-PCR and Western blotting. (**G**). The proliferation ability of HOS transfected with sh-NC, sh-KRT80 (1, 2, 3) was detected by CCK-8. (**H**, **I**). The colony formation ability of HOS transfected with sh-NC, sh-KRT80 (1, 2, 3) was assessed by clone formation assay and the results were counted. *$p<0.05$, **$p<0.01$, ***$p<0.001$. Data were represented as the mean ± SD

provide a novel strategy for osteosarcoma treatment by interfering with its expression.

Discussion

Despite notable advancements, improving survival rates for osteosarcoma patients remains a daunting challenge. The main treatment options for osteosarcoma include neoadjuvant chemotherapy, surgical resection of the primary tumor, and adjuvant chemotherapy. Li has shown that circDOCK1 has regulatory effects on cisplatin sensitivity in vivo and in vitro [6], providing a new solution to the drug resistance of osteosarcoma therapy. Clinical trials have tested various combinations of five chemotherapeutic agents known to be effective in treating osteosarcoma, including methotrexate, doxorubicin, cisplatin, ifosfamide, and etoposide [34–37]. However, no further progress has been reported. Although it is possible to improve survival in recurrent and/or metastatic patients with metastasectomy, the outcome of metastatic patients and those who will exhibit poor response to initial therapy remains unpromising [38–40]. Several studies have suggested that inhibitors targeting transcriptional regulation are essential in effectively treating osteosarcoma [41, 42]. Research has demonstrated that super-enhancers activate relevant genes dependent on cancer cells that promote tumor development [43, 44]. Tumor cells are more dependent on SE-driven transcriptional regulation than normal cells [45]. Thus, targeting SEs with synthetic inhibitors holds considerable promise as a potential therapeutic approach for malignant tumors, such as osteosarcoma.

Inhibitors targeting SEs in general are mainly designed to disrupt SE-related components. These SE inhibitors can be categorized based on the different protein components within the regulatory pathway, including BRD4 inhibitors, CDK inhibitors, histone acetylation inhibitors, and gene editing technologies [46, 47]. The first three are small-molecule inhibitors that effectively block the interaction of SEs with complexes and therefore have greater research value [48]. The inhibitors that have been extensively studied are JQ1 (BRD4 inhibitor) [49], THZ1 (CDK7 inhibitor) [50], THZ531 (CDK12 inhibitor) [51] and TSA (H3K27ac inhibitor) [52], and some of them targeting the SE-related components such as samuraciclib (CDK7 inhibitor) have achieved good results in phase 1 clinical trials and are now in phase 2 clinical trials [53]. In this study, we described a BRD4 inhibitor, GNE-987, that interferes with transcription initiation and elongation. As a core component of the SE complex, BRD4 can bind transcribed oncogenes by recruiting p-TEFb and activating RNA- pol II, which in turn promotes tumor initiation and progression [54]. Based on our tissue microarray immunohistochemistry results, we hypothesized that high BRD4 expression is associated with osteosarcoma, and therefore further experiments were designed to validate the feasibility and efficiency of GNE-987 as an OS cell inhibitor.

Proteolysis targeting chimera (PROTAC) technology has emerged as one of the most promising strategies for new drug discovery. These small-molecule inhibitors offer enhanced precision and efficacy compared to traditional protein inhibitors in the targeted treatment of tumors. GNE-987, as a PROTAC, has been demonstrated to degrade BRD4 in vitro more efficiently than the standard PROTACs, such as MZ1 [27]. GNE-987 has exhibited notable therapeutic potential in hematological tumors, neuroblastomas, and gliomas [29, 55, 56]. However, its role in osteosarcoma is unknown. In this study, we found that GNE-987 induced cell cycle arrest and promoted apoptosis in a time- and dose-dependent manner, which in turn inhibited the proliferation of OS cells.

The VHL Cullin RING E3 ligase is an essential enzyme in the ubiquitin-proteasome system that recruits substrates for the hypoxia-inducible factor for ubiquitination and subsequent proteasomal degradation [57]. The development of PROTACs relied heavily on the design of high-quality small-molecule ligands with enhanced binding affinity for E3 ligases. We further found that knockdown or overexpression of VHL resulted in reduced and increased sensitivity of HOS cells to GNE-987, respectively, and treatment with MG132 partially restored the degradation of BRD4 by GNE-987. The above data suggest that GNE-987 inhibits OS cell proliferation by inducing BRD4 degradation through VHL-mediated proteasomal degradation. Several studies have shown that subcutaneous xenograft tumor experiments in mice can effectively predict drug efficacy in patients [58]. Therefore, we examined the efficacy of GNE-987 in treating OS in mice by using a subcutaneous xenograft model in nude mice. We found that GNE-987 treatment significantly reduced BRD4 and thus inhibited tumor growth. Importantly, the nude mice exhibited no significant side effects or pathological changes in the lungs, livers, and kidneys. The above results suggested that GNE-987 targets BRD4 degradation and exerts anti-tumor effects on OS in vitro and in vivo, which may have some reference value for the clinical treatment of GNE-987.

In order to explore the potential mechanism of GNE-987 against OS, we detected the changes in total transcripts in HOS cells treated with GNE-987 for 24 h by RNA-seq. This analysis piloted us to identify differentially expressed pathways in HOS that were closely associated with cancer characteristics, such as "HALLMARK_G2M_CHECKPOINT" and "HALLMARK_APOPTOSIS". Previous studies have shown that SEs induce hyperactivation of transcriptionally regulated genes, so we identified SE-related oncogenes in HOS cells after integrative analysis of RNA-seq and ChIP-seq

data. Among them were transcription factors such as LIF, RUNX2, and EGFR [31–33], which play important roles in osteosarcoma survival, as well as oncogenes that have rarely been reported in OS. To further narrow down the candidate genes, we performed H3K27ac ChIP-seq on four OS cell lines of OS. Through a comprehensive analysis of various bioinformatics data and functional experiments, we selected an important oncogene that promotes the progression of osteosarcoma: KRT80. KRT80 has been shown to have a high expression status in a variety of tumors and it plays an important role in cancer cell biology, such as eschar. KRT80 has been proven to be highly expressed in a variety of tumors and to play an important role in the biological functions of cancer cells, such as esophageal squamous cell carcinoma [59], colorectal carcinoma [60], gastric cancer [61], non-small cell lung cancer [62] and breast cancer [63]. We found that GNE-987 reduced H3K27ac enrichment at KRT80 by analyzing H3K27ac ChIP-seq. In addition, our results showed that knockdown of the KRT80 gene inhibited the proliferation of OS cells, which is consistent with results from other tumors [64].

Conclusions

Taken together, our findings have demonstrated that GNE-987 selectively degrades BRD4 and blocks the transcription of SE-regulated oncogenes to reduce OS cell proliferation. GNE-987 exerted its excellent antitumor effects by triggering cell cycle arrest and inducing apoptosis. In addition, we identified highly activated and tumor-specific oncogenes by combinatorial bioinformatics analysis. However, it is important to note that our analysis primarily focused on unraveling the mechanism underlying cell proliferation phenotypes. Further investigations are warranted to comprehensively screen and elucidate the roles of oncogenes associated with OS metastasis. Our results suggested that GNE-987 holds promise as an effective therapeutic strategy against OS, and the screened KRT80 may also be a promising target for OS treatment.

Supplementary Information

The online version contains supplementary material available at https://doi.org/10.1186/s12885-024-12691-y.

Supplementary Material 1

Supplementary Material 2

Supplementary Material 3

Supplementary Material 4

Supplementary Material 5

Supplementary Material 6

Supplementary Material 7

Acknowledgements
Not applicable.

Author contributions
D.W: Conceptualization, data curation, formal analysis, methodology, writing-original draft. H.Y: Validation, investigation, writing-review and editing. C.Y: Investigation, writing-review and editing. Z.Z: Data curation, formal analysis, methodology. F.F: Formal analysis, methodology. J.W: Resources, validation. X.L: Resources, methodology. Y.X: Resources, methodology. X.H: Resources, methodology. R.Z: Validation, methodology. Y.C: Validation, visualization. J.Y: Validation, visualization. T.L: Validation, visualization. G.L: Conceptualization, visualization, writing-review and editing. J.P: Conceptualization, resources, supervision, funding acquisition, writing-review and editing. All authors read and approved the final manuscript.

Funding
This work was supported by grants from the National Natural Science Foundation (82141110, 82072767, 81970163, 81971867); Natural Science Foundation of Jiangsu Province (BK20220047); Jiangsu Province's science and technology support program (Social Development) project (BE2021657, BE2021654, BE2022732); National Key R&D Program of China (2022YFC2502702); Suzhou Health Talent Training Project (GSWS2020047, GSWS2021028); the Science and Technology Development Project of Suzhou City (SKJY2021109, SKJY2021111, SKJY2021112, SKY202217 0, SKY2022175, SKY2022182); National Outstanding Youth Cultivation Program Project (YYJQ004) and Jiangsu Provincial Health Commission Scientific Research Project (ZD2022056, Z2022031).

Data availability
The data that support the findings of this study are available on reasonable request from the corresponding author. RNA-seq and ChIP-seq data have been submitted to the GEO database with Accession Number GSE243673.

Declarations

Ethics approval and consent to participate
The Animal Care Committee of Soochow University approved all animal studies (approval number: CAM-SU-AP#: JP-2018-1). All experimental methods were conducted in accordance with the Animal Care and Use Regulations of China. The study is reported in accordance with ARRIVE guidelines (https://arriveguidelines.org).

Consent for publication
All the authors have read and agreed to submit the manuscript to Cancer Cell International with equal responsibility.

Competing interests
The authors declare no competing interests.

Received: 6 November 2023 / Accepted: 24 July 2024
Published online: 01 August 2024

References

1. Choi JH, Ro JY. The 2020 WHO classification of tumors of bone: an updated review. Adv Anat Pathol. 2021;28(3):119–38.
2. Gill J, Gorlick R. Advancing therapy for osteosarcoma. Nat Rev Clin Oncol. 2021;18(10):609–24.
3. Bacci G, et al. High grade osteosarcoma of the extremities with lung metastases at presentation: treatment with neoadjuvant chemotherapy and simultaneous resection of primary and metastatic lesions. J Surg Oncol. 2008;98(6):415–20.
4. Liao D, et al. Chromosomal translocation-derived aberrant Rab22a drives metastasis of osteosarcoma. Nat Cell Biol. 2020;22(7):868–81.
5. Matsuoka K, et al. Wnt signaling and Loxl2 promote aggressive osteosarcoma. Cell Res. 2020;30(10):885–901.
6. Li S, et al. CircDOCK1 promotes the tumorigenesis and cisplatin resistance of osteogenic sarcoma via the miR-339-3p/IGF1R axis. Mol Cancer. 2021;20(1):161.

7. Li S. The basic characteristics of extracellular vesicles and their potential application in bone sarcomas. J Nanobiotechnol. 2021;19(1):277.
8. Mohammad HP, Barbash O, Creasy CL. Targeting epigenetic modifications in cancer therapy: erasing the roadmap to cancer. Nat Med. 2019;25(3):403–18.
9. Fang F, et al. Super-enhancer profiling identifies novel critical and targetable cancer survival gene LYL1 in pediatric acute myeloid leukemia. J Exp Clin Cancer Res. 2022;41(1):225.
10. Zhao J, et al. SIRT7 regulates hepatocellular carcinoma response to therapy by altering the p53-dependent cell death pathway. J Exp Clin Cancer Res. 2019;38(1):252.
11. Chen D, et al. Discovery, structural insight, and bioactivities of BY27 as a selective inhibitor of the second bromodomains of BET proteins. Eur J Med Chem. 2019;182:111633.
12. Stathis A, Bertoni F. BET Proteins as targets for Anticancer Treatment. Cancer Discov. 2018;8(1):24–36.
13. Shu S, et al. Response and resistance to BET bromodomain inhibitors in triple-negative breast cancer. Nature. 2016;529(7586):413–7.
14. Donati B, Lorenzini E, Ciarrocchi A. BRD4 and Cancer: going beyond transcriptional regulation. Mol Cancer. 2018;17(1):164.
15. Latif AL, et al. BRD4-mediated repression of p53 is a target for combination therapy in AML. Nat Commun. 2021;12(1):241.
16. Rahnamoun H, et al. RNAs interact with BRD4 to promote enhanced chromatin engagement and transcription activation. Nat Struct Mol Biol. 2018;25(8):687–97.
17. Faivre EJ, et al. Selective inhibition of the BD2 bromodomain of BET proteins in prostate cancer. Nature. 2020;578(7794):306–10.
18. Zheng ZZ, et al. Super-enhancer-controlled positive feedback loop BRD4/ERalpha-RET-ERalpha promotes ERalpha-positive breast cancer. Nucleic Acids Res. 2022;50(18):10230–48.
19. Shi C, et al. BRD4 as a therapeutic target for nonfunctioning and growth hormone pituitary adenoma. Neuro Oncol. 2020;22(8):1114–25.
20. Liu HJ, et al. Glutathione-scavenging nanoparticle-mediated PROTACs delivery for targeted protein degradation and amplified Antitumor effects. Adv Sci (Weinh). 2023;10(16):e2207439.
21. Wang L, et al. BRD4 inhibition suppresses cell growth, migration and invasion of salivary adenoid cystic carcinoma. Biol Res. 2017;50(1):19.
22. Majumder P et al. A super enhancer controls expression and chromatin architecture within the MHC class II locus. J Exp Med, 2020. 217(2).
23. Vaharautio A, Taipale J. Cancer. Cancer by super-enhancer. Science. 2014;346(6215):1291–2.
24. Li GH, et al. Super-enhancers: a new frontier for epigenetic modifiers in cancer chemoresistance. J Exp Clin Cancer Res. 2021;40(1):174.
25. Tasdemir N, et al. BRD4 connects enhancer remodeling to Senescence Immune Surveillance. Cancer Discov. 2016;6(6):612–29.
26. Suzuki HI, Young RA, Sharp PA. Super-enhancer-mediated RNA Processing revealed by Integrative MicroRNA Network Analysis. Cell. 2017;168(6):1000–e101415.
27. Pillow TH, et al. Antibody conjugation of a chimeric BET degrader enables in vivo activity. ChemMedChem. 2020;15(1):17–25.
28. Sternicki LM, et al. Native Mass Spectrometry for the study of PROTAC GNE-987-Containing Ternary complexes. ChemMedChem. 2021;16(14):2206–10.
29. Chen YL, et al. BRD4 inhibitor GNE987 exerts anti-cancer effects by targeting super-enhancers in neuroblastoma. Cell Biosci. 2022;12(1):33.
30. Nilashi M, et al. A predictive method for hepatitis disease diagnosis using ensembles of neuro-fuzzy technique. J Infect Public Health. 2019;12(1):13–20.
31. Lu B, et al. Epigenetic profiling identifies LIF as a Super-enhancer-controlled Regulator of Stem Cell-like Properties in Osteosarcoma. Mol Cancer Res. 2020;18(1):57–67.
32. Kim YI, et al. SOX9 is a key component of RUNX2-regulated transcriptional circuitry in osteosarcoma. Cell Biosci. 2023;13(1):136.
33. Linder M et al. EGFR is required for FOS-dependent bone tumor development via RSK2/CREB signaling. EMBO Mol Med, 2018. 10(11).
34. Meyers PA, et al. Osteosarcoma: the addition of muramyl tripeptide to chemotherapy improves overall survival–a report from the children's Oncology Group. J Clin Oncol. 2008;26(4):633–8.
35. Marina NM, et al. Comparison of MAPIE versus MAP in patients with a poor response to preoperative chemotherapy for newly diagnosed high-grade osteosarcoma (EURAMOS-1): an open-label, international, randomised controlled trial. Lancet Oncol. 2016;17(10):1396–408.
36. Ferrari S, et al. Neoadjuvant chemotherapy with methotrexate, cisplatin, and doxorubicin with or without ifosfamide in nonmetastatic osteosarcoma of the extremity: an Italian sarcoma group trial ISG/OS-1. J Clin Oncol. 2012;30(17):2112–8.
37. Gaspar N, et al. Results of methotrexate-etoposide-ifosfamide based regimen (M-EI) in osteosarcoma patients included in the French OS2006/sarcome-09 study. Eur J Cancer. 2018;88:57–66.
38. Gaspar N, et al. Lenvatinib with etoposide plus ifosfamide in patients with refractory or relapsed osteosarcoma (ITCC-050): a multicentre, open-label, multicohort, phase 1/2 study. Lancet Oncol. 2021;22(9):1312–21.
39. Daw NC, et al. Recurrent osteosarcoma with a single pulmonary metastasis: a multi-institutional review. Br J Cancer. 2015;112(2):278–82.
40. Briccoli A, et al. High grade osteosarcoma of the extremities metastatic to the lung: long-term results in 323 patients treated combining surgery and chemotherapy, 1985–2005. Surg Oncol. 2010;19(4):193–9.
41. Shi C, et al. PROTAC induced-BET protein degradation exhibits potent anti-osteosarcoma activity by triggering apoptosis. Cell Death Dis. 2019;10(11):815.
42. Lee DH, et al. Synergistic effect of JQ1 and rapamycin for treatment of human osteosarcoma. Int J Cancer. 2015;136(9):2055–64.
43. Jiang YY, et al. Targeting super-enhancer-associated oncogenes in oesophageal squamous cell carcinoma. Gut. 2017;66(8):1358–68.
44. Zhang J, et al. Targeting super-enhancer-associated oncogenes in Osteosarcoma with THZ2, a covalent CDK7 inhibitor. Clin Cancer Res. 2020;26(11):2681–92.
45. Wang X, Cairns MJ, Yan J. Super-enhancers in transcriptional regulation and genome organization. Nucleic Acids Res. 2019;47(22):11481–96.
46. Hnisz D, et al. Super-enhancers in the control of cell identity and disease. Cell. 2013;155(4):934–47.
47. Zheng C, Liu M, Fan H. Targeting complexes of super-enhancers is a promising strategy for cancer therapy. Oncol Lett. 2020;20(3):2557–66.
48. See YX, Wang BZ, Fullwood MJ. Chromatin Interactions and Regulatory Elements in Cancer: from bench to Bedside. Trends Genet. 2019;35(2):145–58.
49. Feng M, et al. The BRD4 inhibitor JQ1 augments the antitumor efficacy of abemaciclib in preclinical models of gastric carcinoma. J Exp Clin Cancer Res. 2023;42(1):44.
50. Cheng ZJ, et al. THZ1 suppresses human non-small-cell lung cancer cells in vitro through interference with cancer metabolism. Acta Pharmacol Sin. 2019;40(6):814–22.
51. Wang C, et al. CDK12 inhibition mediates DNA damage and is synergistic with sorafenib treatment in hepatocellular carcinoma. Gut. 2020;69(4):727–36.
52. Kawasaki K, et al. Chromosome Engineering of Human Colon-derived organoids to develop a model of traditional serrated adenoma. Gastroenterology. 2020;158(3):638–e6518.
53. Coombes RC, et al. Dose escalation and expansion cohorts in patients with advanced breast cancer in a phase I study of the CDK7-inhibitor samuraciclib. Nat Commun. 2023;14(1):4444.
54. Jang MK, et al. The bromodomain protein Brd4 is a positive regulatory component of P-TEFb and stimulates RNA polymerase II-dependent transcription. Mol Cell. 2005;19(4):523–34.
55. Sang X et al. BRD4 Inhibitor GNE-987 Exerts Anticancer Effects by Targeting Super-Enhancer-Related Gene LYL1 in Acute Myeloid Leukemia. J Immunol Res, 2022. 2022: p. 7912484.
56. Ma L, et al. An inhibitor of BRD4, GNE987, inhibits the growth of glioblastoma cells by targeting C-Myc and S100A16. Cancer Chemother Pharmacol. 2022;90(6):431–44.
57. Diehl CJ, Ciulli A. Discovery of small molecule ligands for the Von Hippel-Lindau (VHL) E3 ligase and their use as inhibitors and PROTAC degraders. Chem Soc Rev. 2022;51(19):8216–57.
58. Zanella ER, Grassi E, Trusolino L. Towards precision oncology with patient-derived xenografts. Nat Rev Clin Oncol. 2022;19(11):719–32.
59. Wada M, et al. RNA sequencing-based microRNA expression signature in esophageal squamous cell carcinoma: oncogenic targets by antitumor mir-143-5p and mir-143-3p regulation. J Hum Genet. 2020;65(11):1019–34.
60. Li C, et al. Keratin 80 promotes migration and invasion of colorectal carcinoma by interacting with PRKDC via activating the AKT pathway. Cell Death Dis. 2018;9(10):1009.
61. Song H, et al. CircPIP5K1A activates KRT80 and PI3K/AKT pathway to promote gastric cancer development through sponging miR-671-5p. Biomed Pharmacother. 2020;126:109941.
62. Sanada H et al. Involvement of dual strands of miR-143 (mir-143-5p and miR-143-3p) and their target oncogenes in the Molecular Pathogenesis of Lung Adenocarcinoma. Int J Mol Sci, 2019. 20(18).

63. Perone Y, et al. SREBP1 drives keratin-80-dependent cytoskeletal changes and invasive behavior in endocrine-resistant ERalpha breast cancer. Nat Commun. 2019;10(1):2115.
64. Wei XY, et al. Characters of KRT80 and its roles in neoplasms diseases. Cancer Med. 2023;12(13):13991–4003.

Publisher's Note

Springer Nature remains neutral with regard to jurisdictional claims in published maps and institutional affiliations.